Observation of Shock Waves in a Strongly Interacting Fermi Gas

J. A. Joseph, J. E. Thomas, M. Kulkarni, and A. G. Abanov

Observation of shock waves in a strongly interacting Fermi gas

J. A. Joseph[1] and J. E. Thomas[1]

[1]*Department of Physics, Duke University, Durham, North Carolina, 27708, USA*

M. Kulkarni[2,3] and A. G. Abanov[2]

[2]*Department of Physics and Astronomy, Stony Brook University, Stony Brook, NY 11794-3800, USA and*
[3]*Department of Condensed Matter Physics and Material Science,*
Brookhaven National Laboratory, Upton, NY-11973, USA

We study collisions between two strongly interacting atomic Fermi gas clouds. We observe exotic nonlinear hydrodynamic behavior, distinguished by the formation of a very sharp and stable density peak as the clouds collide and subsequent evolution into a box-like shape. We model the nonlinear dynamics of these collisions using quasi-1D hydrodynamic equations. Our simulations of the time-dependent density profiles agree very well with the data and provide clear evidence of shock wave formation in this universal quantum hydrodynamic system.

Fermi gases with magnetically tunable interactions provide a new universal medium for studies of nonlinear hydrodynamics in quantum matter. Near a collisional (Feshbach) resonance, where the s-wave scattering length diverges, a bias magnetic field can continuously tune the cloud from a weakly interacting molecular Bose-Einstein condensate to a weakly interacting Fermi gas, i.e., the so-called BEC-BCS crossover. At resonance, a Fermi gas is the most strongly interacting non-relativistic system known [1]. It exhibits anisotropic hydrodynamic expansion [2] or "elliptic flow," in common with a quark-gluon plasma [3, 4], a state of matter that existed microseconds after the Big Bang and recently recreated in gold ion collisions. Further, both systems have an extremely low (quantum) viscosity [5] and nearly the same ratio of shear viscosity to entropy density, just a few times the conjectured lower bound for a perfect fluid [6].

In this Letter, we report the observation of shock waves in a strongly interacting Fermi gas. Shock waves are of recent interest in non-equilibrium electron Fermi gases [7, 8] and occur generally in hydrodynamic systems when regions of high density move with a faster local velocity than regions of low density, resulting in increasingly large density gradients. In the absence of dissipative or dispersive forces, this process leads to a "gradient catastrophe," where the density develops infinite gradients. We find that a gradient catastrophe is avoided in a strongly interacting Fermi gas by dissipative forces, which we model as arising from the local shear viscosity. The data are well fit with a kinetic viscosity $10\,\hbar/m$, where m is the atom mass [9].

In contrast, previous experiments on nonlinear hydrodynamics in quantum matter have focused on weakly interacting Bose-Einstein condensates (BECs) [10]. There, the mean field and quantum pressure (i.e., the Gross-Pitaevski equation) lead to dispersive shock waves, characterized by density oscillations [11–13]. For BECs, dispersive shock waves produce soliton trains [14], which

also have been observed and modeled for rapidly rotating BECs [15] and for merging and splitting BECs [16]. Recently, quantum turbulence has been observed in BECs, by using oscillating potentials [17, 18].

Our experiments employ a 50:50 mixture of the two lowest hyperfine states of ^{6}Li, confined in a cigar-shaped CO_2 laser trap, and bisected by a blue-detuned beam at 532 nm, which produces a repulsive potential. The gas is then cooled via forced evaporation near a broad Feshbach resonance at 834 G [19]. After evaporation, the trap is adiabatically recompressed to 0.5% of the initial trap depth. This procedure produces two spatially separated atomic clouds, containing a total of $\simeq 10^5$ atoms per spin state. In the absence of the blue-detuned beam, the trapping potential is cylindrically symmetric with a radial trap frequency of $\omega_x = \omega_y = \omega_\perp = 2\pi \times 437$ Hz and an axial trap frequency of $\omega_z = \sqrt{\omega_{Oz}^2 + \omega_{Mz}^2} = 2\pi \times 27.7$ Hz, where the axial frequency of the optical trap is $\omega_{Oz} = 2\pi \times 18.7$ Hz and $\omega_{Mz} = 2\pi \times 20.4$ Hz arises from curvature in the bias magnetic field. When the repulsive potential is abruptly turned off, the two clouds accelerate toward each other and collide in the CO_2 laser trap. After a chosen hold time, the CO_2 laser is turned off, allowing the atomic cloud to expand for 1.5 ms, after which it is destructively imaged with a 5 μs pulse of resonant light.

Fig. 1 shows false color absorption images for a collision of the atomic clouds at different times after the blue-detuned beam is extinguished. Two distinctive features are clearly seen in this data: (i) the formation of a central peak, which is well-pronounced and robust; (ii) the evolution of this peak into a box-like shape with very sharp boundaries, which propagates outward. The observed large density gradients provide strong evidence of shock wave formation in this system, where the sharp boundaries of the "box" are identified as shock wave fronts. Numerical modeling of the hydrodynamic theory for one dimensional motion is used to predict the evolution of
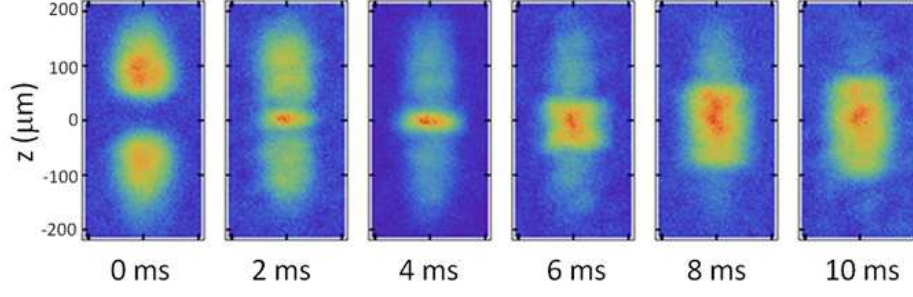
FIG. 1: Collision between two strongly interacting Fermi gas clouds in a cigar-shaped optical trap. The clouds are initially separated by a repulsive 532 nm optical beam. After the 532 nm beam is extinguished (0 ms), the clouds approach each other. False color absorption images show the spatial profiles versus time. Initially, a sharp rise in density occurs in the center of the collision zone. At later times the region of high density evolves from a "peak-like" shape into a "box-like" shape as the shock front propagates outward. The well defined edges of the central zone in the last four images provide evidence of shock wave formation in the strongly interacting Fermi-gas.

the atomic density, yielding profiles in good agreement with the data.

For simplicity, we assume that the cloud is a strongly interacting Fermi gas at zero temperature, i.e., we model the cloud as a single fluid, consistent with our measurements of the sound velocity [20]. In this case, the local chemical potential has the universal form $\mu(n_{3D}) = (1 + \beta)\epsilon_F(n_{3D})$, where $\epsilon_F(n_{3D}) = \frac{\hbar^2}{2m}(3\pi^2 n_{3D})^{2/3}$ is the ideal gas local Fermi energy corresponding to the three-dimensional density n_{3D}. Here, $\beta = -0.61$ is a universal scale factor [2, 21, 22].

Neglecting viscous forces, the dynamics for the density $n_{3D}(\mathbf{r}, t)$ and the velocity field $\mathbf{v}(\mathbf{r}, t)$, are described by the continuity equation,

$$\partial_t n_{3D} + \nabla \cdot (n_{3D}\mathbf{v}) = 0 \qquad (1)$$

and the Euler equation,

$$m\partial_t \mathbf{v} + \nabla \left[\mu(n_{3D}) + U_{trap}(r, z) + \frac{1}{2}m\mathbf{v}^2 \right] = 0, \qquad (2)$$

where we assume irrotational flow. Here $U_{trap}(\mathbf{r}) = \frac{1}{2}m\omega_\perp^2 r^2 + \frac{1}{2}m\omega_z^2 z^2$ is the confining harmonic potential of the cigar-shaped trap.

To determine the initial density profile for the separated clouds, we consider the equilibrium 3D density of the Fermi gas in the trap, including a knife-shaped repulsive potential $V_{rep}(z)$. A blue-detuned laser beam is shaped by a cylindrical lens telescope, i.e., the spot size is small compared to the long dimension of the cigar-shaped cloud and large compared to the transverse dimension. Therefore, the repulsive potential varies only in the z (axial) direction, $V_{rep}(z) = V_0 \exp\left(-(z - z_0)^2/\sigma_z^2\right)$. We measure the width $\sigma_z = 21.2\,\mu\text{m}$. The offset $z_0 = 5\,\mu\text{m}$ of the focus from the center in the long direction of the optical trap is determined by a fit to the first density profile at 0 ms. Using the beam intensity and the

ground state static polarizability of ^{6}Li at 532 nm, we find $V_0 = 12.7\,\mu\text{K}$. The initial density profile is then

$$n_{3D}(r, z) = \tilde{n}\left(1 - \frac{r^2}{R_\perp^2} - \frac{z^2}{R_z^2} - \frac{V_{rep}(z)}{\mu_G}\right)^{\frac{3}{2}}, \qquad (3)$$

where $\tilde{n} = [(2m\mu_G/\hbar^2)/(1 + \beta)]^{3/2}/(3\pi^2)$. In Eq. 3, $R_{z,\perp} = \sqrt{2\mu_G/(m\omega_{z,\perp}^2)}$ and μ_G is the global chemical potential, which is determined by normalizing the integral of the 3D density to the total number N of atoms in both spin states. For $N = 2 \times 10^5$, we find $\mu_G = 0.53\,\mu\text{K}$, $R_z = 220\,\mu\text{m}$, and $R_\perp = 14\,\mu\text{m}$.

We note that $\mu_G/(\hbar\omega_\perp) = 27$, which means that the typical number of filled energy levels of transverse quantization is large. Therefore, in this paper we use 3D hydrodynamics, Eqs. 1 and 2, and neglect effects of transverse quantization even though they are more pronounced in regions with lower density.

We model the dynamics for the one-dimensional motion in the long direction of the cigar-shaped trap. Just after the blue-detuned beam is extinguished, the initial 1D density profile is determined by integrating n_{3D} of Eq. 3 over the transverse dimension r,

$$n_{1D}(z) = \frac{2\pi}{5}R_\perp^2 \tilde{n}\left(1 - \frac{z^2}{R_z^2} - \frac{V_{rep}(z)}{\mu_G}\right)^{\frac{5}{2}}. \qquad (4)$$

In the following we assume that during the evolution the r dependence of Eq. 3 is preserved with the effective size of the cloud being a slow function of z and t. We also assume that the hydrodynamic velocity is along z axis and does not depend on r. Then the subsequent time evolution of the density follows the quasi-1D nonlinear

hydrodynamic equations:

$$\partial_t n = -\partial_z (nv) \tag{5}$$

$$\partial_t v = -\partial_z \left(\frac{v^2}{2} + C n^{\frac{2}{5}} + \frac{1}{2}\omega_z^2 z^2 \right) + \nu \frac{\partial_z(n\partial_z v)}{n}, \tag{6}$$

where $C = \frac{1}{2}\omega_\perp^2 l_\perp^2 \left(\frac{15\pi}{2}l_\perp\right)^{2/5}(1+\beta)^{3/5}$ and $l_\perp = \sqrt{\hbar/(m\omega_\perp)}$ is the oscillator length. For brevity, we have omitted the subscript $1D$ in Eqs. 5 and 6. The last "viscosity" term in Eq. 6 is added *phenomenologically* to describe dissipative effects. For the strongly interacting 1D fluid, ν is the effective kinematic viscosity, which has a natural scale $\hbar/m$. It is the only fitting parameter in the theory [9].

For our previous sound wave experiments [20], we observed nonlinear (amplitude dependent) propagation without shock waves. By reducing the density perturbation, we observed linear propagation. In this regime, one can expand the differential equations (5) and (6) around an equilibrium density configuration $n_0(z)$ in a harmonic trap. Defining $n(z,t) \equiv n_0(z) + \delta n(z,t)$, the linearized evolution equation for $\delta n(z,t)$ (neglecting viscosity) is

$$\partial_t^2 \delta n = \partial_z \left[n_0 \partial_z \left(\frac{2C}{5m} n_0^{-\frac{3}{5}} \delta n \right) \right]. \tag{7}$$

With a flat background density, i.e., constant n_0, with $\mu_G = C n_0^{2/5}$, Eq. 7 reduces to $\partial_t^2 \delta n = c^2 \partial_z^2 \delta n$ with the sound velocity $c = \sqrt{2\mu_G/5m}$, in agreement with predictions [23, 24].

To compare the numerical solutions of Eqs. 5 and 6 with experiment, we note that the images are taken after an additional free expansion for 1.5 ms, during which n_{1D} continues to slowly evolve in the axial potential of the bias magnetic field, i.e., $\omega_z \to \omega_{Mz} = 2\pi \times 20.4$ Hz. We assume that during this expansion, the transverse density profiles keep the same form, but the radius increases with time. Then $n_{3D}(r,z) \to n_{3D}(r/b_\perp, z)/b_\perp^2$, where $b_\perp(t)$ is a transverse scale factor, which obeys $\ddot{b}_\perp = \omega_\perp^2 b_\perp^{-7/3}$, with $b_\perp(0) = 1$ and $\dot{b}_\perp(0) = 0$ [2, 25, 26]. Since the 3D pressure scales as $n_{3D}^{5/3}$, the 1D pressure scales as $b_\perp^{-4/3}$. This leads to a simple modification of Eq. 6: $C \to C(t) = C/b_\perp^{4/3}(t)$.

We numerically integrate Eqs. 5 and 6 using the measured values of the trap frequencies, atom number, and the offset, depth, and width of the repulsive potential. In the numerical simulation we create and load a density array as well as a velocity array with grid spacing δ_z. The initial velocity is set to zero. The simulation then updates the density and velocity field in discrete time steps δ_t according to Eqs. 5 and 6. The 1D density profiles are calculated as a function of time after the repulsive potential is extinguished. Fig. 2 shows the predictions and the data, which are in very good agreement. For the simulation curves shown in the figure we use a

grid of 150 points. To check for numerical consistency, we also employ a smoothed-particle-hydrodynamics [27] approach, where the fluid is described by discrete pseudo-particles. The results obtained indeed coincide with the discretized-grid approach described above.
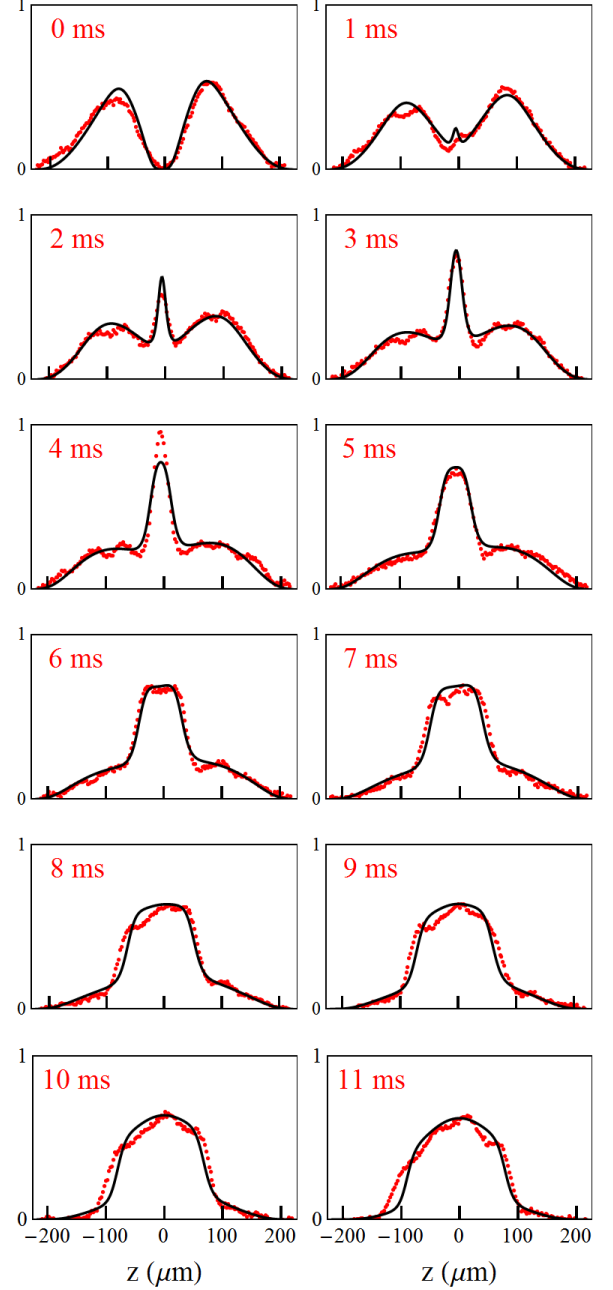

FIG. 2: 1D density profiles divided by the total number of atoms versus time for two colliding strongly interacting Fermi gas clouds. The normalized density is in units of $10^{-2}/\mu$m per particle. Red dots show the measured 1D density profiles. Black curves show the simulation, which uses the measured trap parameters and the number of atoms, with the kinetic viscosity as the only fitting parameter.

As shown in Fig. 2, we observe a dramatic evolution

for the density of the gas. During the collision, a distinct and stable density peak forms at the point of collision in the center of the trap [28]. The density gradient at the side of the central peak increases from its onset until ≈ 3 ms, at which point the gradient reaches its maximum value. A large gradient at the edge of the collision zone is maintained throughout the rest of the experiment. For most of the data, we find relatively small deviations from the simulation. The largest deviation occurs at 4 ms, where the maximum density of the observed central peak exceeds that of the simulation by $\simeq 20\%$.

The steep density gradients observed in Fig. 1 suggest shock wave formation. A deeper analysis of the simulation curves provides additional evidence for shock waves. Without any dissipation, the numerical integration of the quasi-1D theory breaks down due to a "gradient catastrophe." We find that the dissipative force in Eq. 6, which is described by the kinematic viscosity coefficient ν, is required to attenuate the large density gradients and avoid gradient catastrophe. For the data shown in Fig. 2, we find that the best fits are obtained with the viscosity parameter $\nu = 10\,\hbar/m$. For smaller values of ν, the simulation produces qualitatively similar results to those shown in the figure, only with steeper density gradients at the edges of the collision zone. The dissipative term $\propto \nu$ has a relatively small effect on the density profiles, unless we are in a shock wave regime, where the density gradients are large. Hence, the numerical model suggests that the large density gradient observed at the edge of the collision zone is the leading edge of a dissipative shock wave.

Our one-dimensional data for a strongly interacting Fermi gas are very well described by a model based on dissipative nonlinear quantum hydrodynamics. The model employs an effective chemical potential $\mu_{1D} = C\,n_{1D}^{2/5}$, assuming a single fluid near the ground state. However, we expect that at higher temperatures, even in the normal fluid regime, rapid collisional equilibrium in the strongly interacting gas will produce nearly adiabatic evolution with a three-dimensional pressure $\propto n^{5/3}$, and hence an identical power-law dependence for the effective one-dimensional chemical potential. The radial density variations observed in the two dimensional image are not captured in the one-dimensional profiles, but may be studied by expanding the numerical analysis to three dimensions.

In conclusion, we have observed shock waves in a strongly interacting Fermi gas, which provides an entirely new regime for studies of nonlinear wave propagation in cold quantum gases. Studies of nonlinear hydrodynamics can now be done over a wide range of temperatures, in both the superfluid and normal fluid regimes, and magnetic field control of the interaction strength enables continuous tuning from a dispersive BEC to a dissipative Fermi gas. In future work, it will be interesting to study the origin of the effective viscosity, the effects of transverse quantization, and the higher derivative dispersive terms in the stress tensor [7, 8, 11, 29], which become important for large density gradients.

[1] G. Rupak and T. Schäfer, Phys. Rev. A **76**, 053607 (2007).
[2] K. M. O'Hara, S. L. Hemmer, M. E. Gehm, S. R. Granade, and J. E. Thomas, Science **298**, 2179 (2002).
[3] J. E. Thomas, Physics Today pp. 34–37 (2010).
[4] P. F. Kolb and U. Heinz, *Quark Gluon Plasma 3* (World Scientific, 2003), p. 634.
[5] C. Cao, E. Elliott, J. Joseph, H. Wu, J. Petricka, T. Schäfer, and J. E. Thomas, Science **331**, 58 (2010), dOI: 10.1126/science.1195219.
[6] P. K. Kovtun, D. T. Son, and A. O. Starinets, Phys. Rev. Lett. **94**, 111601 (2005).
[7] E. Bettelheim, A. G. Abanov, and P. Wiegmann, Phys. Rev. Lett. **97**, 246401 (2006).
[8] E. Bettelheim, A. G. Abanov, and P. Wiegmann, Phys. Rev. Lett. **97**, 246402 (2006).
[9] In a unitary Fermi gas, which is scale invariant, the bulk viscosity vanishes. We expect that the kinetic viscosity ν arises from the shear viscosity [5], which has a natural scale $\eta \propto \hbar n$, so that $\nu = \eta/(nm) \propto \hbar/m$.
[10] R. Carretero-González, D. J. Frantzeskakis, and P. G. Kevrekidis, Nonlinearity **21**, R139 (2008).
[11] M. A. Hoefer, M. J. Ablowitz, I. Coddington, E. A. Cornell, P. Engels, and V. Schweikhard, Phys. Rev. A. **74**, 023623 (2006).
[12] B. Damski, Phys. Rev. A. **69**, 043610 (2004).
[13] A. M. Kamchatnov, A. Gammal, and R. A. Kraenkel, Phys. Rev. A. **69**, 063605 (2004).
[14] Z. Dutton, M. Budde, C. Slowe, and L. V. Hau, Science **293**, 663 (2001).
[15] T. P. Simula, P. Engels, I. Coddington, V. Schweikhard, E. A. Cornell, and R. J. Ballagh, Phys. Rev. Lett. **94**, 080404 (2005).
[16] J. J. Chang, P. Engels, and M. A. Hoefer, Phys. Rev. Lett. **101**, 170404 (2008).
[17] E. A. L. Henn, J. A. Seman, G. Roati, K. M. F. Magalhães, and V. S. Bagnato, Phys. Rev. Lett. **103**, 045301 (2009).
[18] K. Fujimoto and M. Tsubota, Phys. Rev. A **82**, 043611 (2010).
[19] M. Bartenstein, A. Altmeyer, S. Riedl, R. Geursen, S. Jochim, C. Chin, J. H. Denschlag, R. Grimm, A. Simoni, E. Tiesinga, et al., Phys. Rev. Lett. **94**, 103201 (2005).
[20] J. Joseph, B. Clancy, L. Luo, J. Kinast, A. Turlapov, and J. E. Thomas, Phys. Rev. Lett. **98**, 170401 (2007).
[21] H. Heiselberg, Phys. Rev. A **63**, 043606 (2001).

[22] L. Luo and J. E. Thomas, J. Low Temp. Phys. **154**, 1 (2009).

[23] P. Capuzzi, P. Vignolo, F. Federici, and M. P. Tosi, Phys. Rev. A **73**, 021603(R) (2006).

[24] G. Bertaina, L. Pitaevskii, and S. Stringari, Phys. Rev. Lett. **105**, 150402 (2010).

[25] C. Menotti, P. Pedri, and S. Stringari, Phys. Rev. Lett. **89**, 250402 (2002).

[26] S. Giorgini, L. Pitaevskii, and S. Stringari, Rev. Mod. Phys. **80**, 1215 (2008).

[27] J. Monaghan, Computer Physics Communications **48**, 88 (1988).

[28] In linear hydrodynamics one also observes a peak formation, which can be interpreted as a risidual background in the middle after a small initial dip splits into left and right moving dips (as observed in Ref[[20]]).

[29] R. Meppelink, S. B. Koller, J. M. Vogels, P. van der Straten, E. D. van Ooijen, N. R. Heckenberg, H. Rubinsztein-Dunlop, S. A. Haine, and M. J. Davis, Phys. Rev. A. **80**, 043606 (2009).